Renewable Energy 237 (2024) 121661

Contents lists available at ScienceDirect

Renewable Energy

journal homepage: www.elsevier.com/locate/renene

Relationships between remarkable points in photovoltaic I–V curves

X. Moreno-Vassart [a], F. Javier Toledo [b], Victoria Herranz [b], Vicente Galiano [a,*]

[a] Computers Engineering Department, Miguel Hernández University of Elche, Spain
[b] Center of Operations Research, Miguel Hernández University of Elche, Spain

ARTICLE INFO

Keywords:
Single-diode model
Remarkable points
Key points
Maximum power
Open-circuit point
Short-circuit point

ABSTRACT

In this work we reveal certain intrinsic relationships between the remarkable points of an I–V curve of a photovoltaic panel. Specifically, we carry out a thorough statistical study to determine the existing interconnections between the open-circuit and short-circuit points with the maximum power point, which constitute the so-called remarkable points of an I–V curve. To accomplish this, we analyse nearly one million I–V curves from the National Renewable Energy Laboratory database of the US. Although we find out clear generic relationships, we also provide concrete expressions that connect the remarkable points with a high level of confidence for each of the technologies analysed, which implies that the open-circuit and the short-circuit points can be estimated only with information from the solar panel operating in real time near the maximum power point. Specifically, we provide the regression coefficients of the linear relationships, as well as empirical bounds covering 95% of the samples for the distributions of the ratios between the remarkable points. The results indicate the high reliability of the given estimates.

1. Introduction

Photovoltaics (PV) is a field of research and technology that deals with the conversion of light energy from the sun into electrical energy. Solar energy has become increasingly popular in recent years due to the growing concern for the environment and the need to reduce reliance on fossil fuels. Photovoltaics has emerged as a key technology in this regard, offering a clean, renewable and reliable source of energy. PV panel modelling has become a crucial tool to predict the panel behaviour and maximise its energy production. One of the most widely used models in the literature, due to its relatively simple handling, is the single-diode model (SDM). Fig. 1 is an example of real voltage-current data from a PV panel and a theoretical curve, coming from the SDM, that adjusts these data. Knowing the parameters of the SDM, whose characteristic curve fits the measured data of a panel, allows for example, to predict the behaviour of the panel under other temperature and irradiance conditions [1–4] and, therefore, to know the maximum power point (MPP) of the panel under these other conditions, which results in maximising energy production. As we will see a little later in the introduction, the knowledge of the SDM parameters also allows the panel's operating point to be adjusted in real time around the maximum power point with the so-called MPP tracking algorithms (MPPT).

Predicting the behaviour of solar panels can also be a key tool to detect failures in the systems that govern their operation. For example, if the data measured by a panel at a specific time provides information that contradicts the information given by the manufacturer in the panel's technical datasheet, we can assume the system is failing, which could be caused by a broken electronic component, by shadows on the panels, or by the simple aging of the panel.

The *remarkable points*, also called *notable points*, consisting on the maximum power point $MPP = (V_{MPP}, I_{MPP})$, the short-circuit point $SCP = (0, I_{SC})$ and the open-circuit point $OCP = (V_{OC}, 0)$, are also indicated in Fig. 1. These points, measured in standard test conditions[1] (STC) and in nominal operating cell temperature[2] (NOCT), are part of the technical information that solar panel manufacturers provide in their datasheets. Many works try to obtain from the SDM a single I–V curve by using the remarkable points in STC but, it is known (see [5,6]) that with only these three points there are infinitely many possible SDM I–V curves that cross the three points and also satisfy the slope condition in the MPP given by $I'_{MPP} = -I_{MPP}/V_{MPP}$. Therefore, to obtain a single curve using only the remarkable points, at least one more piece of information would be needed (see again [5,6] to find some particular examples on how to achieve that).

A solar panel working in real conditions can operate in several configurations, the most naive ones, but also the least efficient, work

* Corresponding author.
E-mail addresses: xmoreno-vassart@umh.es (X. Moreno-Vassart), javier.toledo@umh.es (F.J. Toledo), mavi.herranz@umh.es (V. Herranz), vgaliano@umh.es (V. Galiano).

[1] Irradiance 1000 W/m^2 and temperature 25 °C.
[2] Irradiance 800 W/m^2 and temperature 20 °C.

https://doi.org/10.1016/j.renene.2024.121661
Received 21 May 2024; Received in revised form 7 October 2024; Accepted 19 October 2024
Available online 28 October 2024

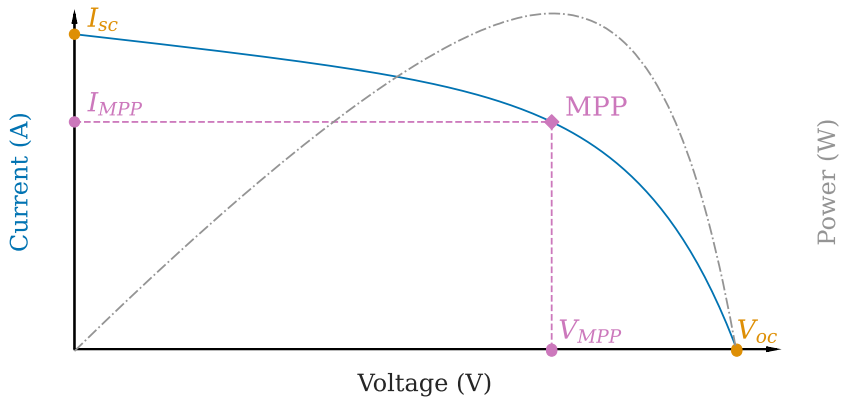

Fig. 1. Sample of I–V curve with corresponding P–V curve and remarkable points.

at a prefixed point, for example that where the panel obtains its maximum performance on average or at a certain time of the day. The most efficient configurations, although the most complex, use MPP tracking (MPPT) algorithms that try to maintain the panel operating at its maximum power at all possible times (see, for example, the MPPT techniques review articles [7–9], and [10]). In this last type of configurations, despite the fact that there is continuous monitoring of the panel, only data close to the MPP are available, and thus, it is not possible to obtain the other remarkable points, the SCP and the OCP, of the panel in real time, information that is relevant in the modelling of the panel and in the analysis of its behaviour. Please note that to obtain the SCP or OCP, the solar panel has to be set in its extreme conditions which, in addition to leaving the panel without generating power, could endanger the system. Therefore, it is evident that being able to predict the values of SCP and OCP only with the MPP could be of great support in the modelling of a solar panel in real time.

Despite the difficulties of knowing the open-circuit voltage or the short-circuit current in real working conditions, there are MPPT algorithms that use these data to predict the maximum power point, these are the so-called Fractional Open-Circuit Voltage (OCV) and Fractional Short-Circuit Current (SCC) methods [11–14]. These methods are based on the assumption that the voltage at the maximum power point is proportional to the open circuit voltage, and that the current at the maximum power point is proportional to the short circuit current. The proportionality constant is key in both methods, although usually only provided in approximate intervals in which the constant is found, without studying the confidence of these intervals in depth. Some reliable relationships can be found in the literature, for example, $2/3 I_{SC} \leq I_{MPP}$ [6] deduced from the data provided in the 8835 modules included in the Energy Commission's Solar Equipment Lists, but it is only a bound in a unique direction. In any case, the existence of the Fractional OCV or SCC methods is also a good rationale for the in-depth study of the relationships between the remarkable points.

The objective of this work is to demonstrate the existence of relationships between the MPP, and the SCP and OCP, and also estimate with the greatest possible precision and reliability the formulas that quantify these relationships. Possible dependencies on factors such as the environmental conditions or the type of panel technology will be analysed. The statistical analysis will be done on the data provided by the National Renewable Energy Laboratory (NREL) of United States [15] which have been obtained on approximately one million curves measured from solar panels in different locations and environmental conditions. The NREL, formerly known as Solar Energy Research Institute, was established in 1974 and is the national laboratory of the U.S. Department of Energy.

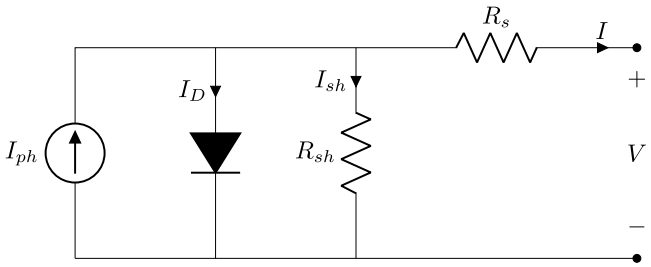

Fig. 2. Electrical circuit associated to the PV single-diode model cell.

2. Preliminaries

In this section we introduce the basic concepts and tools necessary for the development of this study.

Although there are several physical models capable of simulating the behaviour of a PV panel, in this work we use the single-diode model, usually named by the acronym SDM, due to its balance between accuracy and simplicity. The SDM, also called five-parameter model, has been used extensively to better understand and represent the state of a PV panel at a given time, that is, for a given illumination and temperature. Fig. 2 shows the equivalent circuit associated to the SDM.

If we have a PV panel with n_s cells connected in series, after applying the Kirchoff's current law, one obtains the equation

$$I = I_{ph} - I_{sat}\left(\exp\left(\frac{V + I\ R_s}{n_s n V_T}\right) - 1\right) - \frac{V + I\ R_s}{R_{sh}} \tag{1}$$

where the 5 parameters appearing in the previous equation are:

- I_{ph}: photocurrent [A]
- I_{sat}: diode reverse saturation current [A]
- R_s: series resistance [Ω]
- R_{sh}: shunt resistance [Ω]
- n: diode ideality factor

The thermal voltage V_T present in Eq. (1) is given by

$$V_T = \frac{kT}{q} \tag{2}$$

where T is the temperature in Kelvin degrees, $k = 1.3806488 \times 10^{-23}$ J/K the Boltzmann's constant, and $q = 1.60217653 \times 10^{-19}$ C the electron charge.

In many implementations, the number of cells in series n_s, the ideality factor n and the thermal voltage V_T are combined into a single variable/parameter a, specifically

$$a = n_s n V_T \tag{3}$$

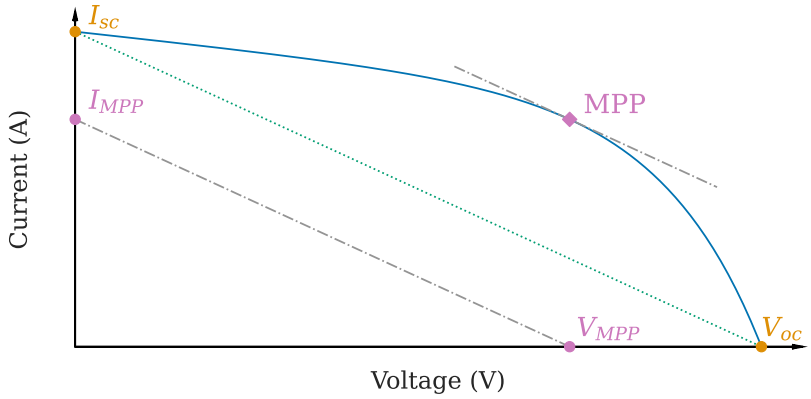

Fig. 3. Slope at the MPP versus Mean Slope between Short-Circuit and Open-Circuit Points.

So, Eq. (1) can be rewritten in a more compact way as

$$I = I_{ph} - I_{sat}\left(\exp\left(\frac{V + I\ R_s}{a}\right) - 1\right) - \frac{V + I\ R_s}{R_{sh}} \tag{4}$$

The SDM has been widely tested and shown to be accurate, that is, it is able to adjust the measured voltage-current data from a solar panel with relatively small errors and using different metrics. This is feasible under a minimum of illumination, above one-half AM1 [16], although it is sometimes valid even for lower illumination.

Multiple algorithms have been developed to extract the SDM parameters with great accuracy, i.e. with parameters whose associated I–V curve fits precisely the measured experimental data of the panel at constant environmental conditions such as [17–20], by minimising the current distance, or [21] by minimising the Euclidean distance.

Besides the parameters, there are several key points that are often mentioned when comparing or characterising I–V curves [22], we will shortly present the short-circuit current, the open-circuit voltage, and the maximum power point, which are usually called the remarkable points of an I–V curve.

- The short-circuit current, I_{SC}, is the maximum current that is produced by a PV panel that is exposed to solar radiation. This current corresponds to a 0Ω load and a voltage of 0 V.
- The open-circuit voltage, V_{OC}, is defined as the maximum voltage that the PV panel can produce with an infinite load and $0A$ current.
- The maximum power point, MPP, with coordinates (V_{MPP}, I_{MPP}), is the point at which a PV panel produces the maximum power output.

The I_{SC}, V_{OC}, and MPP depend on several factors, including the solar cell's design, the amount of light received, the temperature of the solar cell [3,23], but also the age and the corresponding degradation of the cell [24,25]. This means that the point where the solar panel produces the maximum power output changes over time and should be monitored to maximise the power output.

Manufacturers typically provide all 3 remarkable points measured under standard test conditions (STC).

One important well-known property, that is derived from the MPP of an I–V curve, is the fact that the derivative of current with respect to the voltage at this point can be expressed only in terms of the MPP coordinates I_{MPP} and V_{MPP}. We know that power function is given by $P = IV$, and thus, its derivative with respect to V at the MPP is $P'_{MPP} = I'_{MPP}V_{MPP} + I_{MPP}$. Since P has a relative maximum at the MPP, indeed a global maximum, then $P'_{MPP} = 0$, and therefore, the slope of the I–V curve at the MPP is given by

$$I'_{MPP} = \left.\frac{\mathrm{d}I}{\mathrm{d}V}\right|_{MPP} = -\frac{I_{MPP}}{V_{MPP}}. \tag{5}$$

Another interesting characteristic of the I–V curve that we will manage throughout this study is the mean slope of the I–V curve, that is, the slope of the segment that joins $(0, I_{SC})$ and $(V_{OC}, 0)$. We will call it I'_{MSP} which is simply given by

$$I'_{MSP} = -\frac{I_{SC}}{V_{OC}}. \tag{6}$$

Fig. 3 helps with the geometrical interpretation of both I'_{MPP} (the slope of the dash-dotted line, the tangent at the MPP) and I'_{MSP} (the slope of the dotted segment).

In this work we will use the so-called Two-Step Linear Least-Squares (TSLLS) method, provided in [19], to obtain the SDM parameters (I_{ph}, I_{sat}, a, R_s, R_{sh} from Eq. (4)), since it has been proven to be one of the fastest and most accurate extraction methods, and in addition, only requires 5 or more points of the I–V curve and is not tied to the prior knowledge and accuracy of I_{SC}, V_{OC}, I_{MPP}, or V_{MPP}. The TSLLS method finds the quintet of SDM parameters that minimises the root mean square error (RMSE) with respect to the current distance — the difference between the measured intensity and the intensity reconstructed from each proposed parameter set. Once the parameters are obtained, we will calculate the 3 remarkable points corresponding to the theoretical I–V curve by means of the fast and efficient methodologies described in [22].

As commented in the introduction section, this work will explore the relationships between the remarkable points corresponding to the SDM I–V curves obtained from a dataset of around a million I–V curves of the NREL. As one of many lines of research, the NREL has been measuring I–V curves for 8 different technologies and a total of 22 different PV modules across different vendors. They are located not only at their Golden facility but also Eugene, Oregon, and Cocoa, Florida. Some of that data are available to the public for research purposes and was decisive to this study. The public data utilised is comprised of I–V curves, temperature and irradiance readings taken every 5 min [26]. The data covers several years of data, from January 2011 to September 2013.

3. Methodology, results and discussion

3.1. Data under study

The data for this analysis comes from the NREL as explained at the end of the preliminary section. Recall that the initial dataset contains a total of 1025600 curves. The PV modules utilised are comprised of the following technologies (and their contractions as used by the NREL) in alphabetical order:

- Amorphous silicon (a-Si)

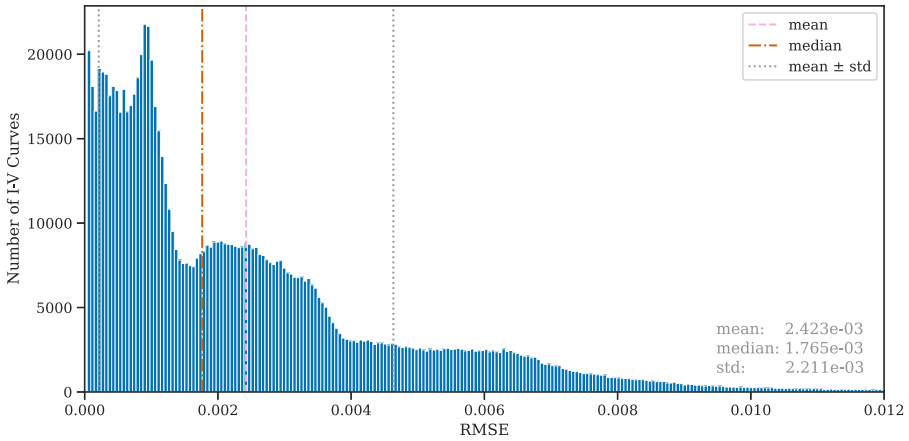

Fig. 4. Distribution of RMSE from TSLLS.

Table 1
PV Modules and their locations, with area measured in squared metres.

Module	I–V curves per city			Area	Ns	Np
	Eugene	Cocoa	Golden			
aSiMicro03036	43 343	39 037	0	1.4200	180	1
aSiTandem72–46	43 266	39 186	0	0.7900	38	1
aSiTriple28324	42 705	38 485	0	1.0100	11	2
CdTe75638	42 248	39 080	0	0.7200	116	1
CIGS8–001	43 146	38 939	0	0.7290	66	2
CIGS39017	42 674	34 775	0	1.7500	72	1
HIT05667	43 271	38 377	0	1.2600	72	1
mSi0166	43 268	36 765	0	0.3429	36	1
mSi0188	43 127	39 102	0	0.3429	36	1
mSi460A8	43 115	38 929	0	0.6470	36	1
xSi12922	43 185	38 990	0	0.6470	36	1
aSiMicro03038	0	0	12 148	1.4200	180	1
aSiTandem90–31	0	0	12 070	0.7900	38	1
aSiTriple28325	0	0	11 445	1.0100	11	2
CdTe75669	0	0	11 953	0.7200	116	1
CIGS1–001	0	0	12 011	0.7290	66	2
CIGS39013	0	0	11 437	1.7500	72	1
HIT05662	0	0	11 876	1.2600	72	1
mSi0247	0	0	11 912	0.3429	36	1
mSi0251	0	0	11 887	0.3429	36	1
mSi460BB	0	0	11 919	0.6470	36	1
xSi11246	0	0	11 929	0.6470	36	1

- Amorphous silicon hybrid tandem (a-Si-tandem)
- Amorphous silicon hybrid triple-junction (a-Si-triple)
- Cadmium Telluride (CdTe)
- Copper Indium Gallium Selenide (CIGS)
- Hetero junction intrinsic thin layer (HIT)
- Monocrystalline silicon (mono-Si)
- Polycrystalline silicon (multi-Si)

Crystalline silicon is the most common PV technology, it makes up 95% of photovoltaic energy production (82% of total from monocrystalline panels and 13% from polycrystalline ones). The remaining 5% is produced by Thin-film panels, mostly comprised of Cadmium Telluride (4.1% of total).

The 22 modules from NREL are distributed unevenly across all three cities as shown in Table 1, with half of them being present in both Eugene and Cocoa and the rest in Golden. Nevertheless, the studied PV technologies are represented in all 3 locations. Table 2 describes geographical details of each site.

3.2. Methodology

The first step is to extract the 5 parameters of each I–V curve with the TSLLS method. Indeed, we will extract the parameters minimising the root mean square error (RMSE) with respect to the current, which is the most commonly used error in the literature [19,27,28]. Fig. 4 shows the distribution of RMSE for all the NREL curves. Curves beyond 3 standard deviations (3.64% of curves) have been discarded because are comprised of curves from shadowed PV panels and with measurement errors.

The second step calculates the 3 remarkable points of each I–V curve, from the SDM parameters, with the methodologies proposed in [22].

The third and final step evaluates the following three linear regressions without vertical intercept:

- $I_{SC} = \alpha_I I_{MPP}$
- $V_{OC} = \alpha_V V_{MPP}$
- $I'_{MSP} = \alpha_S I'_{MPP}$

Regression's fit is evaluated with RMSE (vertical distance between sample and linear regression) and the coefficient of determination (R^2), which is equivalent, in this case, to the square of the Pearson correlation coefficient. The distribution of quotients $\frac{I_{SC}}{I_{MPP}}$, $\frac{V_{OC}}{V_{MPP}}$, and $\frac{I'_{MSP}}{I'_{MPP}}$ are also plotted, displaying a behaviour that might be missed harder to spot only from a scatter plot (Figs. 5(a), 5(c) and 5(e)). Additionally, for each distribution of quotients, a lower and an upper bound are provided, so that the interval they form encloses 95% of samples and its amplitude is the smallest possible.

3.3. Discussion

Firstly, curves from all technologies are considered as a single dataset (Fig. 5). Linear trends are already visible (Figs. 5(b), 5(d) and 5(f)) from this first approach. Fig. 5(a) in particular displays a bimodal distribution with third smaller peak in between. The vertical pink dashed lined through the distribution represents the regression

Table 2
PV modules locations, with latitude and longitude expressed in degrees, elevation in metres, and modules' tilt and azimuth in degrees.

City	State	Time Zone	Latitude	Longitude	Elevation	Module tilt	Module azimuth
Cocoa	Florida	−5	28.39	−80.46	12	28.5	180.0
Eugene	Oregon	−8	44.05	−123.07	145	44.0	180.0
Golden	Colorado	−7	39.74	−105.18	1798	40.0	180.0

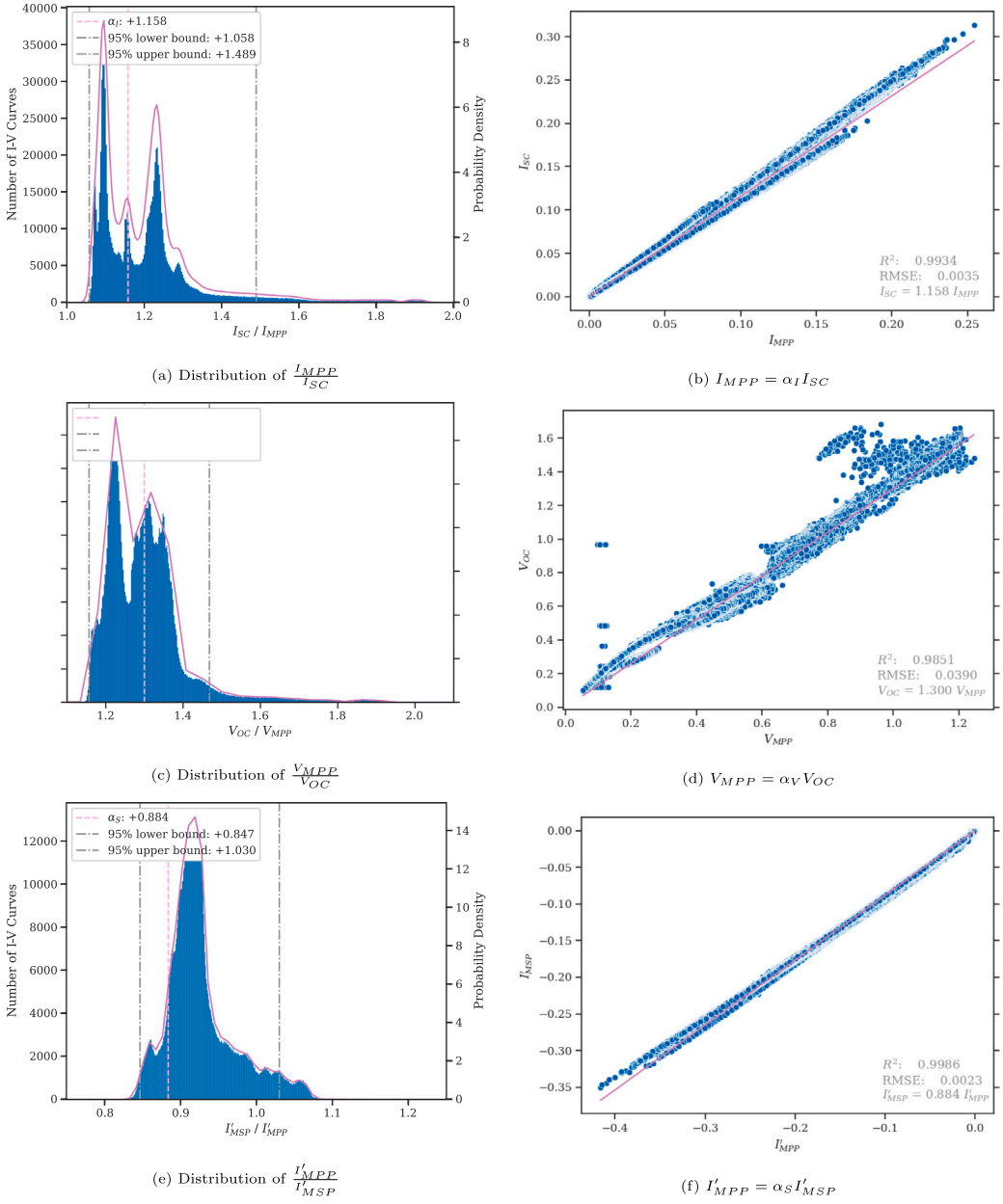

(a) Distribution of $\frac{I_{MPP}}{I_{SC}}$

(b) $I_{MPP} = \alpha_I I_{SC}$

(c) Distribution of $\frac{V_{MPP}}{V_{OC}}$

(d) $V_{MPP} = \alpha_V V_{OC}$

(e) Distribution of $\frac{I'_{MPP}}{I'_{MSP}}$

(f) $I'_{MPP} = \alpha_S I'_{MSP}$

Fig. 5. Distribution of remarkable quotients and regressions — all technologies.

coefficient, while the 95% bounds are shown with dash-dotted grey lines. These observations motivate the analysis on subsamples of the data, first on a per technology basis and, if inconclusive, on a per panel basis.

When treating technologies separately, the bimodal behaviour (see Fig. 5(a)) leaves place to unimodal distributions of the quotient $\frac{I_{SC}}{I_{MPP}}$ (Fig. 6) and displays low dispersion. In fact, the analysis has been repeated on a per module basis with near identical quotient results for modules of the same technology, which justifies grouping them up. CIGS I–V curves are the only notable exception (Fig. 6(e)). For that reason CIGS modules are also treated individually in this study. See also that 25% of samples of CIGS technology do not satisfy the inequality $2/3 I_{SC} \leq I_{MPP}$ from [6].

Fig. 7 shows the resulting regressions for each technology. The values for each technology are available in Table 3a, except CIGS technology (Table 3b). The coefficient of determination of HIT panels is $R^2 = 0.99995$ but appears rounded up.

Figs. 8 and 9 display the aforementioned distribution and regression for $V_{OC} = \alpha_V V_{MPP}$. The regression itself (Fig. 9) shows a higher dispersion for all technologies compared to the previous I_{SC} (Fig. 7), as also illustrated by a lower R^2.

The interval enclosing 95% of the samples of the distribution of $\frac{I_{SC}}{I_{MPP}}$ (Fig. 6) has an amplitude of approximately 10.15% of α_I, with the exception of CIGS I_{MPP}. Besides, the interval amplitude for $\frac{V_{OC}}{V_{MPP}}$ is close to 8.3t % of α_V. In both cases, the small percentage indicates that the distributions of $\frac{I_{SC}}{I_{MPP}}$ and $\frac{V_{OC}}{V_{MPP}}$ are very concentrated. These results support their use (see Table 3a) as more refined estimations, for the proposed technologies, of the inverse of the voltage factor K_{pv} and K_v shared, respectively, in [13,14]. It is also true, with the previous exception, that $2/3 V_{OC} \leq V_{MPP}$.

Finally, the distribution of $\frac{I'_{MSP}}{I'_{MPP}}$ and regression $I'_{MSP} = \alpha_S I'_{MPP}$ are respectively shown in Figs. 10 and 11. We must pay attention to the low dispersion for each technology shown in Fig. 10 where the coefficients

Table 3
Regression coefficients overview.

(a) Regression coefficients per technology

Technology	$I_{SC} = \alpha_I I_{MPP}$					$V_{OC} = \alpha_V V_{MPP}$					$I'_{MSP} = \alpha_S I'_{MPP}$				
	α_I	R^2	RMSE	95% bounds		α_V	R^2	RMSE	95% bounds		α_S	R^2	RMSE	95% bounds	
				Lower	Upper				Lower	Upper				Lower	Upper
a-Si	1.2256	0.9997	0.0000	1.1852	1.2797	1.3428	0.8911	0.0195	1.2924	1.3839	0.9006	0.9998	0.0000	0.8835	0.9597
a-Si-tandem	1.2316	0.9995	0.0002	1.2002	1.3191	1.3179	0.7175	0.0309	1.2751	1.3604	0.9175	0.9994	0.0002	0.9036	0.9962
a-Si-triple	1.2293	0.9997	0.0014	1.1923	1.2851	1.3263	0.6862	0.0251	1.2604	1.3931	0.9035	0.9996	0.0015	0.8887	0.9915
CdTe	1.1612	0.9996	0.0001	1.1467	1.4380	1.3191	0.5089	0.0224	1.2650	1.3994	0.8599	0.9984	0.0002	0.8377	1.0357
CIGS	1.2996	0.9972	0.0013	1.1262	1.8012	1.4079	0.9366	0.0296	1.2319	1.7486	0.9128	0.9961	0.0028	0.8799	1.0625
HIT	1.0732	1.0000	0.0002	1.0609	1.0950	1.1831	0.7345	0.0115	1.1543	1.2310	0.8864	0.9995	0.0008	0.8719	0.9346
multi-Si	1.0951	0.9999	0.0004	1.0828	1.2028	1.2359	0.7691	0.0134	1.1948	1.3174	0.8772	0.9991	0.0019	0.8586	0.9311
mono-Si	1.0939	0.9999	0.0005	1.0781	1.1539	1.2232	0.5720	0.0144	1.1841	1.2881	0.8665	0.9992	0.0024	0.8490	0.9435
all	1.1583	0.9934	0.0035	1.0579	1.4892	1.3000	0.9851	0.0390	1.1569	1.4681	0.8840	0.9986	0.0023	0.8469	1.0302

(b) Regression coefficients for CIGS modules

Module	$I_{SC} = \alpha_I I_{MPP}$					$V_{OC} = \alpha_V V_{MPP}$					$I'_{MSP} = \alpha_S I'_{MPP}$				
	α_I	R^2	RMSE	95% bounds		α_V	R^2	RMSE	95% bounds		α_S	R^2	RMSE	95% bounds	
				Lower	Upper				Lower	Upper				Lower	Upper
CIGS1-001	1.1385	0.9996	0.0001	1.1244	1.3109	1.2635	0.8242	0.0059	1.2262	1.3177	0.8938	0.9986	0.0008	0.8766	0.9991
CIGS8-001	1.2119	0.9953	0.0004	1.1359	1.5802	1.3387	0.4773	0.0208	1.2469	1.6183	0.9307	0.9969	0.0012	0.8960	1.0412
CIGS39013	1.3341	0.9964	0.0017	1.2949	1.8134	1.4560	0.8550	0.0262	1.3684	1.7609	0.9184	0.9932	0.0042	0.8834	1.0689
CIGS39017	1.3009	0.9974	0.0015	1.2670	1.8882	1.4422	0.8971	0.0302	1.3497	1.8586	0.9093	0.9950	0.0036	0.8805	1.0683

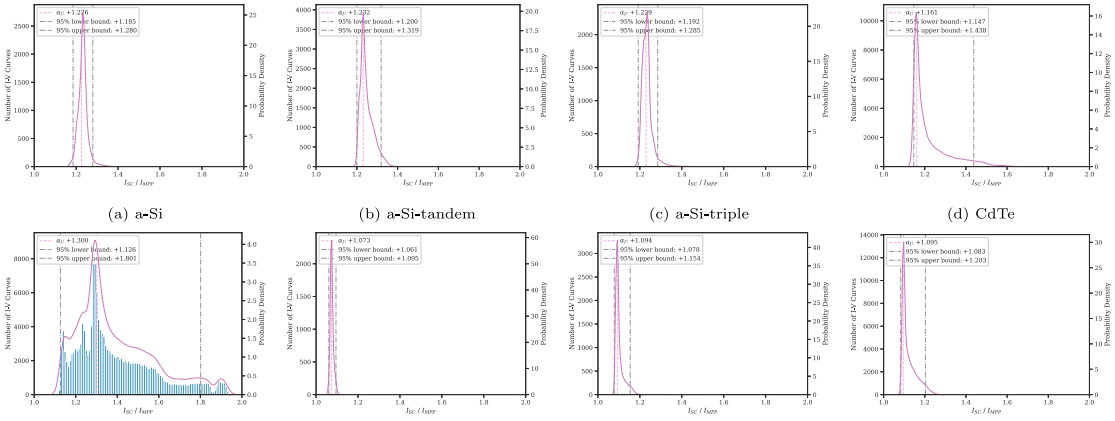

(a) a-Si (b) a-Si-tandem (c) a-Si-triple (d) CdTe

(e) CIGS (f) HIT (g) mono-Si (h) multi-Si

Fig. 6. Distribution of $\frac{I_{MPP}}{I_{SC}}$ per technology.

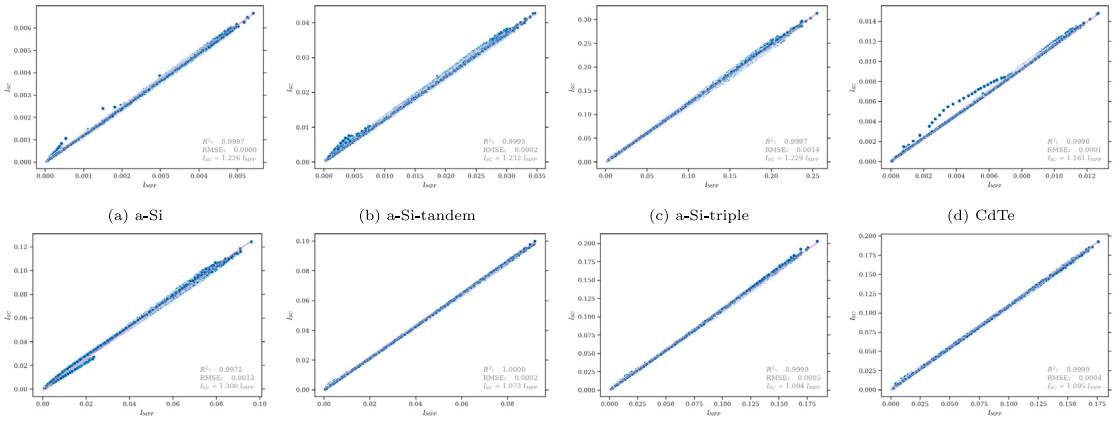

(a) a-Si (b) a-Si-tandem (c) a-Si-triple (d) CdTe

(e) CIGS (f) HIT (g) mono-Si (h) multi-Si

Fig. 7. $I_{SC} = \alpha_I I_{MPP}$ per technology.

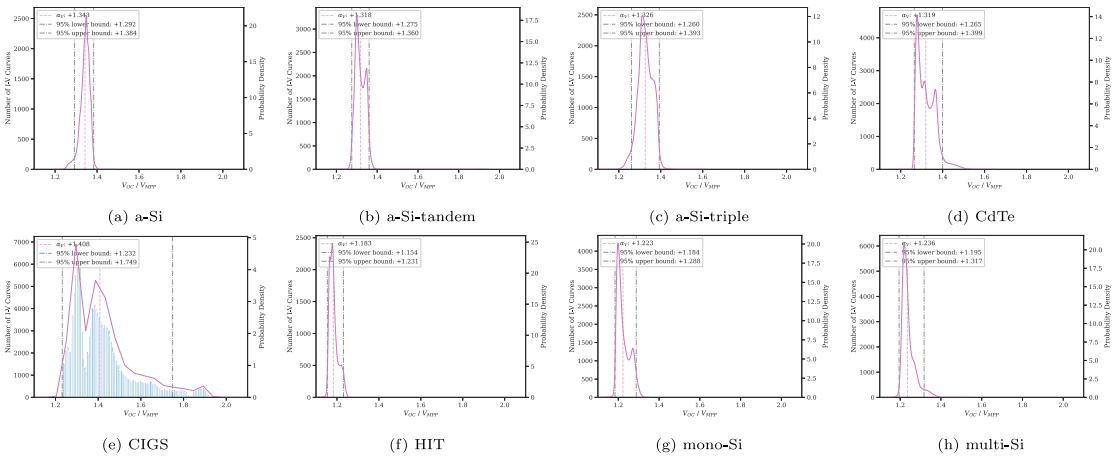

(a) a-Si (b) a-Si-tandem (c) a-Si-triple (d) CdTe

(e) CIGS (f) HIT (g) mono-Si (h) multi-Si

Fig. 8. Distribution of $\frac{V_{MPP}}{V_{OC}}$ per technology.

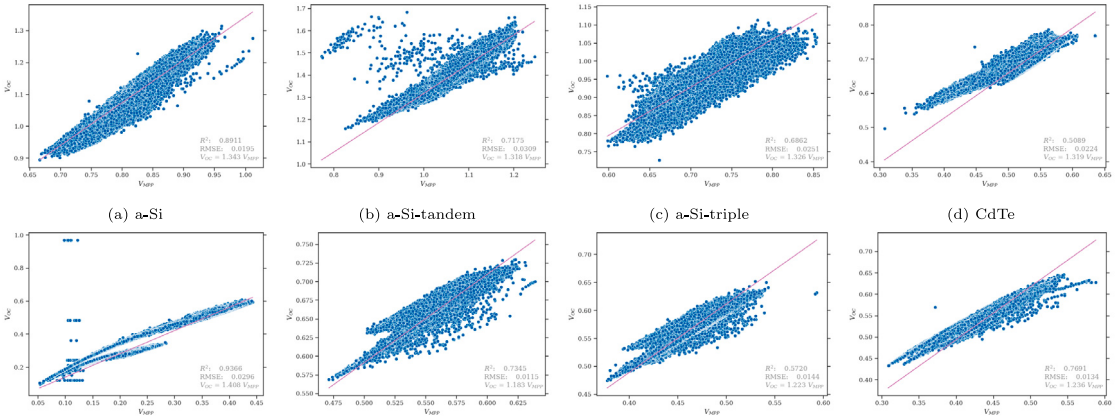

(a) a-Si (b) a-Si-tandem (c) a-Si-triple (d) CdTe

(e) CIGS (f) HIT (g) mono-Si (h) multi-Si

Fig. 9. $V_{OC} = \alpha_V V_{MPP}$ per technology.

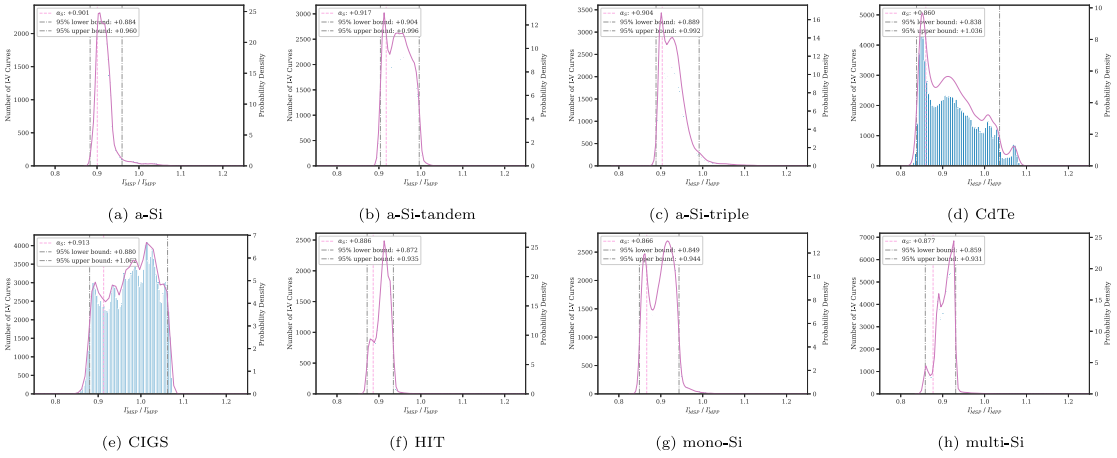

(a) a-Si (b) a-Si-tandem (c) a-Si-triple (d) CdTe

(e) CIGS (f) HIT (g) mono-Si (h) multi-Si

Fig. 10. Distribution of $\frac{I'_{MPP}}{I_{MSD}}$ per technology.

of determination (R^2) are close to the good results obtained for $I_{SC} = \alpha_I I_{MPP}$, with a similarly low dispersion. Now, the amplitude of the interval covering 95% of samples of the $\frac{I'_{MSP}}{I'_{MPP}}$ distribution, including CIGS modules, is 11.3% of α_S. This fact shows that $I'_{MSP} = \alpha_S I'_{MPP}$ is a suitable estimation for all the technologies.

The estimation of V_{OC} from V_{MPP} can benefit from regression with a vertical intercept, as particularly noticeable on Figs. 9(d) and 9(h). Table 4 provides the coefficients for the new regressions. In Table 4a we can observe an improvement of the coefficient of determination (R^2) and RMSE for V_{OC} across all technologies. Nevertheless, the vertical

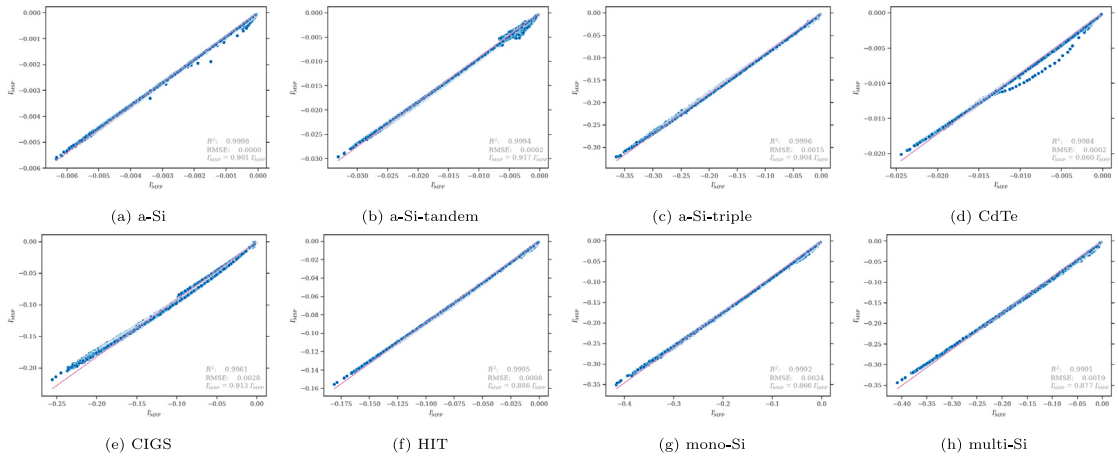

(a) a-Si (b) a-Si-tandem (c) a-Si-triple (d) CdTe

(e) CIGS (f) HIT (g) mono-Si (h) multi-Si

Fig. 11. $I'_{MSP} = \alpha_S I'_{MPP}$ per technology.

Table 4
Regression coefficients overview with vertical intercept.

(a) Regression coefficients with intercept per technology

Technology	$I_{SC} = \beta_{1,I} I_{MPP} + \beta_{0,I}$				$V_{OC} = \beta_{1,V} V_{MPP} + \beta_{0,V}$				$I'_{MSP} = \beta_{1,S} I'_{MPP} + \beta_{0,S}$			
	$\beta_{1,I}$	$\beta_{0,I}$	R^2	RMSE	$\beta_{1,V}$	$\beta_{0,V}$	R^2	RMSE	$\beta_{1,S}$	$\beta_{0,S}$	R^2	RMSE
a-Si	1.2251	0.0000	0.9997	0.0000	1.4464	−0.0870	0.8957	0.0191	0.8943	0.0000	0.9999	0.0000
a-Si-tandem	1.2274	0.0001	0.9995	0.0002	1.1230	0.2125	0.7398	0.0297	0.9059	−0.0002	0.9997	0.0001
a-Si-triple	1.2298	−0.0001	0.9997	0.0014	1.2451	0.0581	0.6891	0.0250	0.8934	−0.0018	0.9998	0.0010
CdTe	1.1493	0.0001	0.9998	0.0001	0.8456	0.2544	0.7428	0.0162	0.8382	−0.0003	0.9995	0.0001
CIGS	1.2883	0.0004	0.9974	0.0013	1.3665	0.0123	0.9376	0.0294	0.8872	−0.0025	0.9977	0.0021
HIT	1.0735	0.0000	1.0000	0.0002	0.9410	0.1343	0.7866	0.0103	0.8762	−0.0008	0.9997	0.0006
multi-Si	1.0892	0.0004	0.9999	0.0003	0.8650	0.1678	0.9434	0.0067	0.8644	−0.0019	0.9995	0.0014
mono-Si	1.0939	0.0000	0.9999	0.0005	0.8359	0.1789	0.7289	0.0115	0.8532	−0.0027	0.9996	0.0016
all	1.1592	−0.0001	0.9934	0.0035	1.3293	−0.0193	0.9856	0.0382	0.8749	−0.0013	0.9989	0.0021

(b) Regression coefficients with intercept for CIGS modules

Module	$I_{SC} = \beta_{1,I} I_{MPP} + \beta_{0,I}$				$V_{OC} = \beta_{1,V} V_{MPP} + \beta_{0,V}$				$I'_{MSP} = \beta_{1,S} I'_{MPP} + \beta_{0,S}$			
	$\beta_{1,I}$	$\beta_{0,I}$	R^2	RMSE	$\beta_{1,V}$	$\beta_{0,V}$	R^2	RMSE	$\beta_{1,S}$	$\beta_{0,S}$	R^2	RMSE
CIGS1-001	1.1205	0.0002	1.0000	0.0000	0.9347	0.0790	0.9411	0.0034	0.8717	−0.0011	0.9996	0.0004
CIGS8-001	1.1738	0.0004	0.9971	0.0003	0.8071	0.1155	0.8591	0.0108	0.9075	−0.0011	0.9979	0.0009
CIGS39013	1.2765	0.0027	0.9994	0.0007	1.0786	0.1313	0.9790	0.0100	0.8685	−0.0063	0.9980	0.0023
CIGS39017	1.2572	0.0020	0.9996	0.0006	1.1237	0.1115	0.9809	0.0130	0.8709	−0.0046	0.9983	0.0021

intercept for I_{SC} and I'_{MSP} regressions, respectively $\beta_{0,I}$ and $\beta_{0,S}$ are close to 0. This justifies the use of Table 3 as a reference and the validity of the 95% bounds for I_{SC} and I'_{MSP}. Table 4b shows significantly different values of $\beta_{1,V}$ and $\beta_{0,V}$ for each different model of CIGS technology, improving the results given in Table 3b.

We would like to point out that the previous results do not depend on the environmental conditions, in particular temperature and irradiance, in which I–V curves have been measured.

4. Conclusions

This study has proved statistical relationships, $I_{SC} = \alpha_I I_{MPP}$, $V_{OC} = \alpha_V V_{MPP}$ and $I'_{MSP} = \alpha_S I'_{MPP}$, which link the MPP to the SCP and the OCP with high correlation regardless of temperature and irradiance, given a minimum of illumination and no partial shading. It is interesting to note that the first and last ones have been particularly strong. We provide not only the regression coefficients, α_I, α_V and α_S, of the linear relationships, but also empirical bounds enclosing 95% of the samples for the distributions of the quotients $\frac{I_{SC}}{I_{MPP}}$, $\frac{V_{OC}}{V_{MPP}}$, and $\frac{I'_{MSP}}{I'_{MPP}}$. We point out that the intervals associated to the previous bounds have a relatively small amplitude with respect to the corresponding regression coefficients. This indicates the high concentration of samples which justifies the reliability of the estimations. Although we have obtained good estimations valid across the PV technology, it has also been observed that the studied relationships are more strongly linked to the physical properties of the panel, and therefore, for greater accuracy, the estimations may require an individual analysis (such as for CIGS modules). So, we recommend replicating the study for a particular PV installation (e.g., a solar farm comprised of a single PV model) and perform an approach fined-tuned per technology that offers a tighter fit than a generic estimator. Based on our analysis performed over more than a million curves of the NREL, we propose the use of Tables 3 and 4 to estimate respectively I_{SC} and V_{OC} from MPP for the panel technology analysed. It would be very interesting to make a study of the relationships analysed in this work, discriminating by the aging of the panels for the same technology. Since this factor influences the values of the remarkable points of the panels, it is expected that the relationships with this casuistry will be stronger for panels with the same aging.

CRediT authorship contribution statement

X. Moreno-Vassart: Writing – review & editing, Writing – original draft, Visualization, Validation, Resources, Methodology, Investigation, Funding acquisition, Data curation, Conceptualization. **F. Javier Toledo:** Writing – review & editing, Writing – original draft, Visualization, Validation, Supervision, Resources, Project administration, Methodology, Investigation, Funding acquisition, Data curation, Conceptualization. **Victoria Herranz:** Writing – review & editing, Writing –

original draft, Visualization, Validation, Supervision, Resources, Project administration, Methodology, Investigation, Funding acquisition, Data curation, Conceptualization. **Vicente Galiano:** Writing – review & editing, Writing – original draft, Visualization, Validation, Supervision, Resources, Project administration, Methodology, Investigation, Funding acquisition, Data curation, Conceptualization.

Declaration of competing interest

The authors declare that they have no known competing financial interests or personal relationships that could have appeared to influence the work reported in this paper.

Acknowledgements

The authors would like to thank the National Renewable Energy Laboratory for providing the I–V curves used in this research.

F. Javier Toledo, V. Galiano and Victoria Herranz were supported by Grant TED2021-130025B-I00 funded by MICIU/AEI/10.13039/501100011033 and by Europen Union NextGenerationEU/PRTR. F. Javier Toledo was supported by Grant PID2022-136399NB-C22 funded by MICIU/AEI/10.13039/501100011033, and by Grant PROMETEO/2021/063 funded by the government of the Valencian Community. V. Galiano's work has received funding from the Valencian Ministry of Innovation, Universities, Science and Digital Society under Grant CIAICO/2021/278 and from Grant PID2021-123627OB-C55 funded by MICIU/AEI/10.13039/501100011033. This work has also been supported by the European Union NextGenerationEU/PRTR.

Data availability

The raw data required to reproduce the above findings are available to download from the National Renewable Energy Laboratory (NREL) database of USA [15].

References

[1] W. De Soto, S. Klein, W. Beckman, Improvement and validation of a model for photovoltaic array performance, Sol. Energy 80 (1) (2006) 78–88, http://dx.doi.org/10.1016/j.solener.2005.06.010, URL https://www.sciencedirect.com/science/article/pii/S0038092X05002410.

[2] K.J. Sauer, T. Roessler, C.W. Hansen, Modeling the irradiance and temperature dependence of photovoltaic modules in pvsyst, IEEE J. Photovolt. 5 (1) (2015) 152–158, http://dx.doi.org/10.1109/JPHOTOV.2014.2364133.

[3] C.S. Ruschel, F.P. Gasparin, A. Krenzinger, Experimental analysis of the single diode model parameters dependence on irradiance and temperature, Sol. Energy 217 (2021) 134–144, http://dx.doi.org/10.1016/j.solener.2021.01.067, URL https://www.sciencedirect.com/science/article/pii/S0038092X21000931.

[4] Y. Hishikawa, M. Yoshita, H. Ohshima, K. Yamagoe, H. Shimura, A. Sasaki, T. Ueda, Temperature dependence of the short circuit current and spectral responsivity of various kinds of crystalline silicon photovoltaic devices, Japan. J. Appl. Phys. 57 (8S3) (2018) 08RG17, http://dx.doi.org/10.7567/JJAP.57.08RG17.

[5] A. Laudani, F. Riganti Fulginei, A. Salvini, Identification of the one-diode model for photovoltaic modules from datasheet values, Sol. Energy 108 (2014) 432–446, http://dx.doi.org/10.1016/j.solener.2014.07.024, URL https://www.sciencedirect.com/science/article/pii/S0038092X14003739.

[6] F. Toledo, J.M. Blanes, V. Galiano, A. Laudani, In-depth analysis of single-diode model parameters from manufacturer's datasheet, Renew. Energy 163 (2021) 1370–1384, http://dx.doi.org/10.1016/j.renene.2020.08.136, URL https://www.sciencedirect.com/science/article/pii/S0960148120313811.

[7] D.P. Hohm, M.E. Ropp, Comparative study of maximum power point tracking algorithms, Prog. Photovolt., Res. Appl. 11 (1) (2003) 47–62, http://dx.doi.org/10.1002/pip.459, URL https://onlinelibrary.wiley.com/doi/abs/10.1002/pip.459.

[8] M.A. Husain, A. Tariq, S. Hameed, M.S.B. Arif, A. Jain, Comparative assessment of maximum power point tracking procedures for photovoltaic systems, Green Energy Environ. 2 (2017) 5–17, http://dx.doi.org/10.1016/j.gee.2016.11.001.

[9] R.B. Bollipo, S. Mikkili, P.K. Bonthagorla, Critical review on pv mppt techniques: Classical, intelligent and optimisation, IET Renew. Power Gener. 14 (9) (2020) 1433–1452, http://dx.doi.org/10.1049/iet-rpg.2019.1163, arXiv:https://ietresearch.onlinelibrary.wiley.com/doi/pdf/10.1049/iet-rpg.2019.1163. URL https://ietresearch.onlinelibrary.wiley.com/doi/abs/10.1049/iet-rpg.2019.1163.

[10] S. Saravanan, N. Ramesh Babu, Maximum power point tracking algorithms for photovoltaic system – a review, Renew. Sustain. Energy Rev. 57 (2016) 192–204, http://dx.doi.org/10.1016/j.rser.2015.12.105, URL https://www.sciencedirect.com/science/article/pii/S1364032115014884.

[11] Y.-P. Huang, A rapid maximum power measurement system for high-concentration photovoltaic modules using the fractional open-circuit voltage technique and controllable electronic load, IEEE J. Photovolt. 4 (6) (2014) 1610–1617, http://dx.doi.org/10.1109/JPHOTOV.2014.2351613.

[12] P. Das, Maximum power tracking based open circuit voltage method for pv system, Energy Procedia 90 (2016) 2–13, http://dx.doi.org/10.1016/j.egypro.2016.11.165, 5th International Conference on Advances in Energy Research (ICAER) 2015. URL https://www.sciencedirect.com/science/article/pii/S1876610216313753.

[13] D. Baimel, S. Tapuchi, Y. Levron, J. Belikov, Improved fractional open circuit voltage mppt methods for pv systems, Electronics 8 (3) http://dx.doi.org/10.3390/electronics8030321, URL https://www.mdpi.com/2079-9292/8/3/321.

[14] A. Hassan, O. Bass, M.A. Masoum, An improved genetic algorithm based fractional open circuit voltage mppt for solar pv systems, Energy Rep. 9 (2023) 1535–1548, http://dx.doi.org/10.1016/j.egyr.2022.12.088, URL https://www.sciencedirect.com/science/article/pii/S2352484722026762.

[15] B. Marion, A. Anderberg, C. Deline, M. Muller, G. Perrin, J. Rodriguez, S. Rummel, T. Silverman, F. Vignola, S. Barkaszi, Data for validating models for pv module performance. http://dx.doi.org/10.21948/1811521.

[16] D. Chan, J. Phillips, J. Phang, A comparative study of extraction methods for solar cell model parameters, Solid-State Electron. 29 (3) (1986) 329–337, http://dx.doi.org/10.1016/0038-1101(86)90212-1, URL https://www.sciencedirect.com/science/article/pii/0038110186902121.

[17] A. Laudani, F. Riganti Fulginei, A. Salvini, High performing extraction procedure for the one-diode model of a photovoltaic panel from experimental i–v curves by using reduced forms, Sol. Energy 103 (2014) 316–326, http://dx.doi.org/10.1016/j.solener.2014.02.014, URL https://www.sciencedirect.com/science/article/pii/S0038092X14000929.

[18] A.A. Cárdenas, M. Carrasco, F. Mancilla-David, A. Street, R. Cárdenas, Experimental parameter extraction in the single-diode photovoltaic model via a reduced-space search, IEEE Trans. Ind. Electron. 64 (2) (2017) 1468–1476, http://dx.doi.org/10.1109/TIE.2016.2615590.

[19] F.J. Toledo, J.M. Blanes, V. Galiano, Two-step linear least-squares method for photovoltaic single-diode model parameters extraction, IEEE Trans. Ind. Electron. 65 (2018) 6301–6308, http://dx.doi.org/10.1109/tie.2018.2793216.

[20] J. Xu, Separable nonlinear least squares search of parameter values in photovoltaic models, IEEE J. Photovolt. 12 (1) (2022) 372–380, http://dx.doi.org/10.1109/JPHOTOV.2021.3126105.

[21] E. Batzelis, J.M. Blanes, F.J. Toledo, V. Galiano, Noise-scaled euclidean distance: A metric for maximum likelihood estimation of the pv model parameters, IEEE J. Photovolt. 12 (3) (2022) 815–826, http://dx.doi.org/10.1109/JPHOTOV.2022.3159390.

[22] F.J. Toledo, V. Galiano, V. Herranz, J.M. Blanes, E. Batzelis, A comparison of methods for the calculation of all the key points of the pv single-diode model including a new algorithm for the maximum power point, Optim. Eng. http://dx.doi.org/10.1007/s11081-023-09850-8.

[23] J.C. Fan, Theoretical temperature dependence of solar cell parameters, Sol. Cells 17 (2) (1986) 309–315, http://dx.doi.org/10.1016/0379-6787(86)90020-7, URL https://www.sciencedirect.com/science/article/pii/0379678786900207.

[24] K.L. Kennerud, Analysis of performance degradation in cds solar cells, IEEE Trans. Aerosp. Electron. Syst. AES-5 (6) (1969) 912–917, http://dx.doi.org/10.1109/TAES.1969.309966.

[25] M. Piliougine, G. Spagnuolo, M.S. de Cardona, Series resistance temperature sensitivity in degraded mono–crystalline silicon modules, Renew. Energy 162 (2020) 677–684, http://dx.doi.org/10.1016/j.renene.2020.08.026, URL https://www.sciencedirect.com/science/article/pii/S0960148120312635.

[26] B. Marion, A. Anderberg, C. Deline, J. del Cueto, M. Muller, G. Perrin, J. Rodriguez, S. Rummel, T.J. Silverman, F. Vignola, R. Kessler, J. Peterson, S. Barkaszi, M. Jacobs, N. Riedel, L. Pratt, B. King, New data set for validating pv module performance models, in: 2014 IEEE 40th Photovoltaic Specialist Conference, PVSC, 2014, pp. 1362–1366, http://dx.doi.org/10.1109/PVSC.2014.6925171.

[27] A. Laudani, F. Mancilla-David, F. Riganti-Fulginei, A. Salvini, Reduced-form of the photovoltaic five-parameter model for efficient computation of parameters, Sol. Energy 97 (2013) 122–127, http://dx.doi.org/10.1016/j.solener.2013.07.031, URL https://www.sciencedirect.com/science/article/pii/S0038092X1300306X.

[28] F.J. Toledo, V. Galiano, J.M. Blanes, V. Herranz, E. Batzelis, Photovoltaic single-diode model parametrization. an application to the calculus of the euclidean distance to an i–v curve, Math. Comput. Simulation http://dx.doi.org/10.1016/j.matcom.2023.01.005, URL https://www.sciencedirect.com/science/article/pii/S0378475423000058.